

Co-Evaporated Perovskite Light-Emitting Transistor Operating at Room Temperature

Maciej Klein, Jia Li, Annalisa Bruno,* and Cesare Soci*

Solution-processed hybrid organic–inorganic perovskite light-emitting transistors (PeLETs) suffer from low brightness and environmental instability induced by temperature-activated trapping, ionic motion, and polarization effects, which so far have been hindering the realization of devices operating at room temperature. Here high quality thermally co-evaporated methylammonium lead iodide perovskite films are employed to minimize ionic motion and significantly improve the electroluminescence characteristics of the perovskite active layer, enabling stable device operation up to ≈ 310 K. The demonstration of PeLETs operating at and beyond room-temperature paves the way for practical applications in the rapidly evolving area of solid-state lighting, active-matrix displays, and visible light communications.

1. Introduction

Over the last decade, hybrid organic–inorganic perovskites (HOIPs) have attracted enormous attention for their unique physical and chemical properties.^[1] A concerted effort of the research community worldwide resulted in the application of hybrid perovskites in a variety of optoelectronic devices including perovskite light-emitting transistors (PeLETs), which combine light emission with electronic switching and amplification.^[2] PeLETs provide a versatile platform to study fundamental transport properties of halide perovskites and for novel system applications such as active matrix displays, electrically pumped lasers, or visible light communication (VLC)—which employs ambient lighting to transmit signals.^[3–5] A high defect tolerance toward electron–hole recombination is often invoked as the main factor behind the excellent performance

of HOIP-based devices. However, the intrinsic transport characteristics of charge carriers in perovskites are severely affected by thermally-activated trapping, ionic motion, and organic cation polarization effects; these factors prevent balanced ambipolar transport at room temperature and affect long-term stability, hindering achievement of theoretical device performance.^[6–8] Various methods to improve solar cell and light-emitting diode (LED) characteristics, such as tuning the perovskite composition,^[9] interface passivation,^[10] or device structure engineering,^[11,12] provided ad hoc optimization of device characteristics. However, these


strategies did not solve the root of the problem: overall poor transport properties and stability of the active materials. As a result, nearly six years after the introduction of the PeLET concept, both conventional perovskite field-effect transistors (FETs) and LETs cannot perform to their full potential.^[5,13] So far, only a few works reported balanced ambipolar transport^[14–17] or light emission from perovskite field-effect transistors,^[2,18–20] indicative of the severe limitations posed by the intrinsic transport and electroluminescence characteristics of HOIP materials.

In our previous work, we demonstrated that light emission from methylammonium lead iodide ($\text{CH}_3\text{NH}_3\text{PbI}_3$, MAPbI₃) transistors driven by pulsed gate or drain voltages is brighter and more uniform than devices operating in conventional DC-driven mode.^[18] Moreover, frequency modulation minimizes ionic vacancy drift and methylammonium cation polarization within the perovskite active layer and enables space-charge, field-assisted charge carrier injection, extending the optimum operating range of the device up to 240 K. Other groups have also shown that transistors employing an $\text{In}_2\text{O}_3/\text{ZnO}$ heterojunction with a self-organized NFPI₇ multiple quantum well perovskite acting as electron transporting layer, and a light-emitting/hole transporting layer, display high field-effect electron mobility ($>20 \text{ cm}^2 \text{ V}^{-1} \text{ s}^{-1}$) and bright light emission (external quantum efficiency EQE $\approx 0.2\%$) at room temperature.^[19] In a different approach, cesium lead bromide (CsPbBr_3) quantum dots sandwiched between poly(9-carbazole) (PVK) hole-transporting layer and ZnO electron-transporting layer were found to exhibit electron mobility of $0.12 \text{ cm}^2 \text{ V}^{-1} \text{ s}^{-1}$ and electroluminescence with EQE of 6.5×10^{-4} , also at room temperature.^[20] However, the latter devices operated in unipolar regime, where relatively high electron mobility was attributed to channel formation in the metal-oxide semiconductors layer, while radiative recombination of charge carriers occurred only in the area under or nearby the hole injecting electrode.

Dr. M. Klein, Prof. C. Soci
Division of Physics and Applied Physics
Nanyang Technological University
Singapore 637371, Singapore
E-mail: csoci@ntu.edu.sg

Dr. M. Klein, Dr. J. Li, Dr. A. Bruno, Prof. C. Soci
Energy Research Institute @ NTU (ERI@N)
Research Techno Plaza
Nanyang Technological University
50 Nanyang Drive, Singapore 637553, Singapore
E-mail: annalisa@ntu.edu.sg

Dr. M. Klein, Prof. C. Soci
Centre for Disruptive Photonic Technologies
TPI, SPMS, Nanyang Technological University
Singapore 637371, Singapore

 The ORCID identification number(s) for the author(s) of this article can be found under <https://doi.org/10.1002/aelm.202100403>.

DOI: 10.1002/aelm.202100403

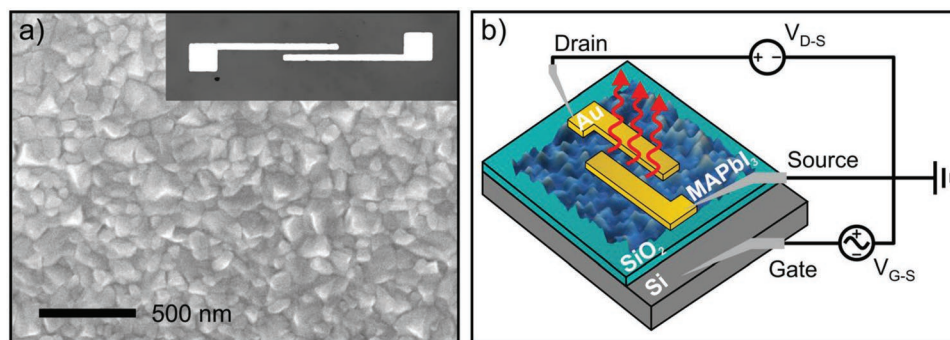


Figure 1. Co-evaporated perovskite light-emitting transistor (PeLET) device structure. a) Top-view SEM image of MAPbI₃ film fabricated by vacuum thermal evaporation. Inset: optical microscope image of the device. b) Schematic architecture and biasing configuration of the bottom-gate, top-contact, AC-driven PeLET. V_{D-S} stands for drain-source bias while V_{G-S} is the gate-source bias.

Significant improvement in operation of single-layer field-effect transistors based on a variety of perovskite compositions was reported recently, highlighting the importance of active materials optimization.^[21,22] Field-effect mobility $>1 \text{ cm}^2 \text{ V}^{-1} \text{ s}^{-1}$ in hysteresis-free and operationally stable devices at room temperature were shown. Nonetheless, those systems were also optimized for unipolar operation regime (n-type or p-type only), and neither ambipolar transport nor light emission could be obtained. Thus, a radically new solution based on better ambipolar materials is needed to achieve more stable and efficient PeLETs operating at room temperature.

Physical vacuum deposition of perovskite thin films offers considerable advantages over solution-processing, such as the intrinsic purity of sublimated materials, homogeneity and reproducibility of the resulting film morphology, and accurate control of the film thickness.^[23] Recent developments with thermally co-evaporated perovskite thin films have shown remarkable improvement in perovskite solar cell characteristics, yielding power conversion efficiencies of 20.28% for small area devices (0.1 cm^2), a record value exceeding 18% for mini-modules,^[24,25] and remarkable thermal and ambient stability.^[26] Expectedly, vapor-based techniques could thus improve the quality of FET active layers and balance charge carrier transport.

In this work, we realized co-evaporated CH₃NH₃PbI₃ perovskite light-emitting field-effect transistors with balanced ambipolar charge injection and improved electroluminescence characteristics at room temperature. While electronic transport in HOIPs is inevitably affected by ionic motion, particularly around room temperature, we find that in high-quality co-evaporated films ionic effects are more effectively mitigated by high-frequency modulation of the bias voltage, improving field-effect gating and extending the operating regime of the PeLETs to room temperature and beyond.

2. Results and Discussion

Details of the co-evaporated perovskite films and the PeLET device architecture used in this study are provided in **Figure 1**. Charge transport and electroluminescence (EL) characteristics of perovskite light-emitting devices are strongly affected by the HOIP film formation and its resulting morphology.^[27] Here we used a CH₃NH₃PbI₃ active layer prepared by the

thermal co-evaporation process of PbI₂ and CH₃NH₃I (methylammonium iodide, MAI). The optimized film deposition procedure^[24] yielded highly uniform, compact, and pin-hole free polycrystalline layers, with mean grain size of $\approx 100 \text{ nm}$ (Figure 1a) and exceptionally smooth surface ($R_{\text{rms}} = 3 \text{ nm}$ as characterized by atomic force microscopy, AFM, topographic imaging, Figure S1, Supporting Information). LET devices were fabricated in top contact, bottom gate configuration (inset of Figure 1a,b)—a device architecture known to improve charge injection and overall device performance.^[18,28]

Typical DC electrical characteristics of the transistors are shown in **Figures 2** and **3**. The transfer characteristics of co-evaporated devices reveal the ambipolar character of charge transport with $I_{\text{on}}/I_{\text{off}} \approx 10^4$ and $I_{\text{on}}/I_{\text{off}} \approx 10$ at $T = 77 \text{ K}$ for n-type and p-type transport, respectively (Figure 2). The corresponding charge carrier mobilities indicate that transport is dominated by electrons at low temperatures and becomes more balanced at room temperature. Field-effect electron (μ_e) and hole (μ_h) mobilities extracted at drain-source voltage $V_{D-S} = \pm 60 \text{ V}$ are $\mu_e = (8.6 \pm 0.6) \times 10^{-2} \text{ cm}^2 \text{ V}^{-1} \text{ s}^{-1}$; $\mu_h = (1.3 \pm 0.3) \times 10^{-4} \text{ cm}^2 \text{ V}^{-1} \text{ s}^{-1}$ at $T = 77 \text{ K}$ and $\mu_e = (7 \pm 6) \times 10^{-6} \text{ cm}^2 \text{ V}^{-1} \text{ s}^{-1}$; $\mu_h = (9 \pm 6) \times 10^{-6} \text{ cm}^2 \text{ V}^{-1} \text{ s}^{-1}$ at $T = 293 \text{ K}$. The large errors affecting room temperature mobility values are typical of high-leakage current devices fabricated from PbI₂ precursor, as noted in previous studies.^[2,18,21,29]

The output characteristics of the PeLETs reveal strong gate modulation of drain current (I_{D-S}) for both n-type and p-type operating regimes (Figure 3). At 77 K, electron characteristics show clear evidence of saturation being reached around $V_{D-S} = 40 \text{ V}$, while hole characteristics do not reach saturation and exhibit an anomalous gating behavior which may be indicative of electron-dominated transport and space charge screening effects. Unlike solution-processed PeFETs operated in DC-driven mode (Figure S3, Supporting Information), the gating effect in co-evaporated PeLETs persists up to 293 K, with the expected drain-source bias dependence for both electrons and holes (although saturation could not be reached within the bias range investigated).

Apparent hysteretic behavior of the current is observed between forward and reverse bias sweeps in both transfer and output characteristics, which is typical of HOIP materials with ionic character, similar to what was observed in spin-coated devices.^[2,7,18,21] The hysteresis reveals the presence of various

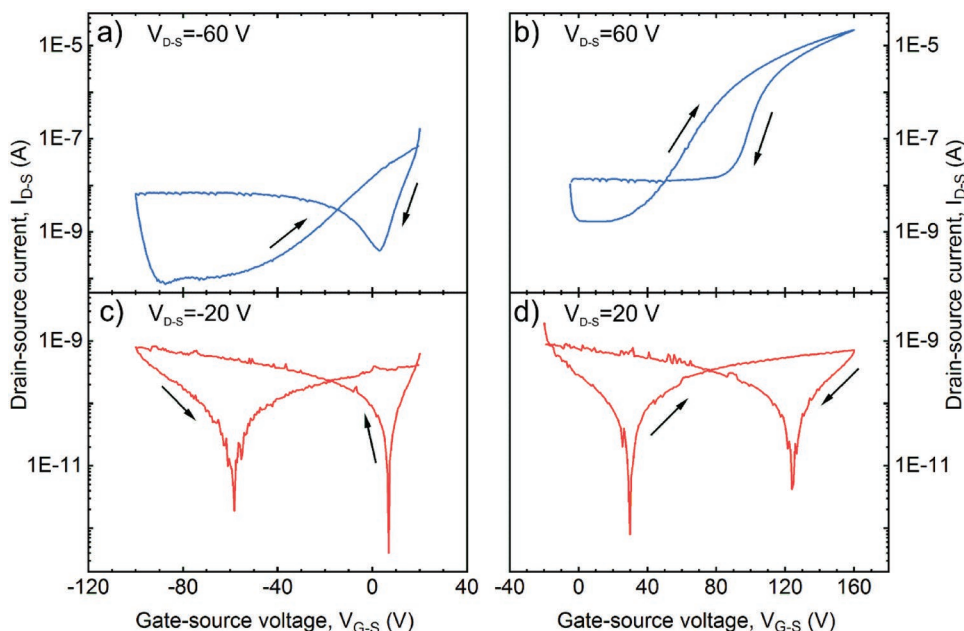


Figure 2. DC electrical transfer characteristics of the PeLET. a,c) p-type and b,d) n-type transfer characteristics measured at 77 K (a,b) and 293 K (c,d) under the constant drain-source bias (V_{D-S}) indicated in the panels. Arrows indicate the gate-source bias (V_{G-S}) sweep direction.

types of ions (I^- anions and methylammonium MA^+ , Pb^{2+} cations originating from vacancies, interstitials, or antisite substitutions) which migrate under the action of the applied gate and drain-source electric fields. Interestingly, n-type output characteristics at 293 K show opposite hysteresis loop direction comparing to other measurements in Figure 3, which suggests that mobile ions of opposite sign have higher activity under such operating conditions. As derived from the analysis of space-charge-limited electron and hole currents in $MAPbI_3$

films, the direction of hysteresis reveals the sign of the dominant mobile ionic species, that is, under p-type operating regime positive ions lead to higher current, while negative ions to lower current, in the forward branch of the hysteresis loop.^[30]

To quantify the extent of ion migration we compare the output characteristics of co-evaporated and solution-processed PeLETs obtained at 293 K in Figures S3,S4, Supporting Information. Under positive gate bias (n-type output curves), the calculated area of the hysteresis loop, S , of co-evaporated devices

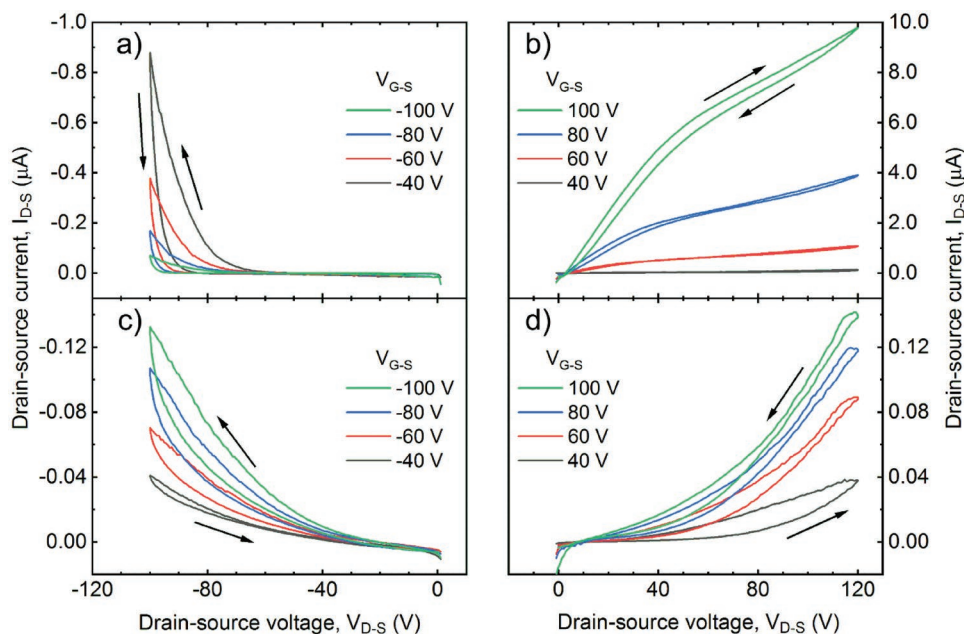


Figure 3. DC electrical output characteristics of PeLETs. a,c) p-type and b,d) n-type output characteristics measured at 77 K (a,b) and 293 K (c,d) under the constant gate-source bias (V_{G-S}) indicated in the panels. Arrows indicate the drain-source bias (V_{D-S}) sweep direction.

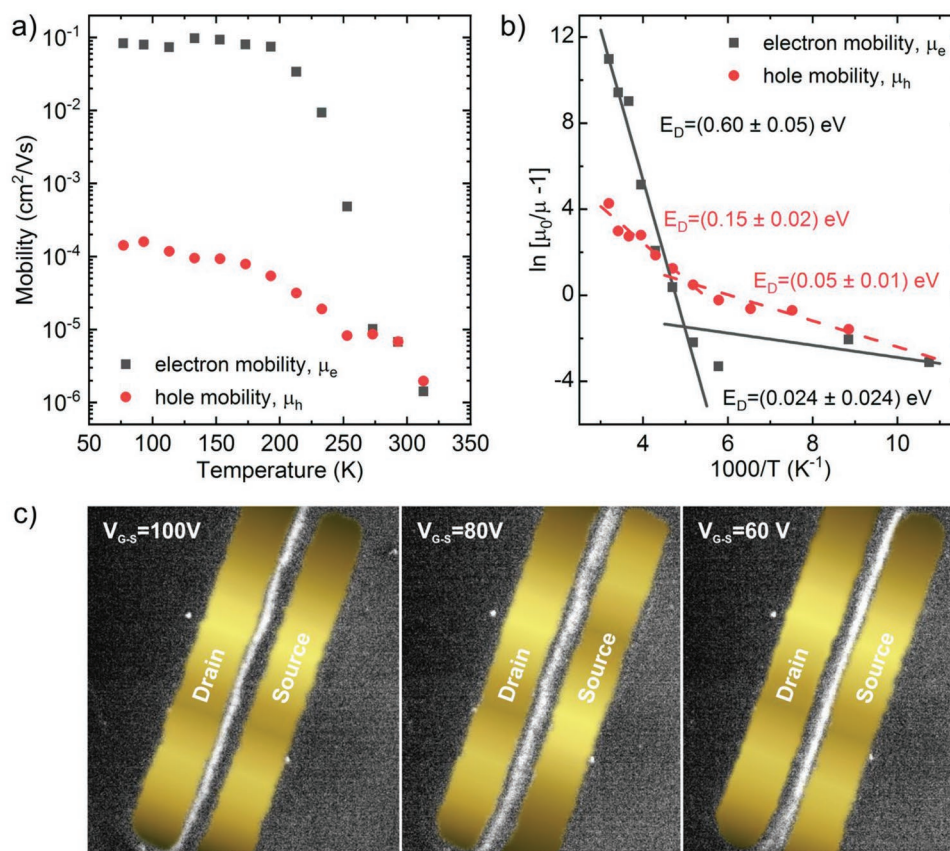


Figure 4. Charge carrier transport and injection characteristics of DC-driven PeLETs. a) Temperature dependence of electron (μ_e) and hole (μ_h) mobilities extracted from the transfer curves with $V_{D-S} = 60$ V and $V_{D-S} = -60$ V, respectively; b) Arrhenius plot of μ_e and μ_h with corresponding deactivation energies in the low and high-temperature regimes (the solid lines show linear fits to the data in the high and low-temperature ranges). c) EL emission recorded at 77 K under an optical microscope with fixed $V_{D-S} = 120$ V, and different gate biases V_{G-S} .

is nearly six times smaller than that of solution-processed devices; conversely, under negative gate bias (p-type output curves), hysteresis values are comparable in the two devices (except for $V_{G-S} = -40$ V which was the first measurement in the series)—see also summary Table S1, Supporting Information. The hysteresis area of co-evaporated devices at both 77 and 293 K is also comparable (Figure S2 and Table S1, Supporting Information). Thus, output characteristics of PeLETs suggest that co-evaporated films are less affected by ionic effects. The reasons behind the reduction of the ion movement in co-evaporated MAPbI₃ films are ascribable to their morphological and structural characteristics. The increase of grain boundaries in smaller grain-size (≈ 100 nm) co-evaporated films, compared to spin-coated films used in previous works (≈ 200 nm),^[18] may inhibit the movement of ions, as previously found in other films.^[31] On the other hand, the absence of tensile stress in co-evaporated MAPbI₃ may also contribute to the reduction of MA⁺ movement under voltage bias.^[26,32]

The temperature dependence of the extracted field-effect charge carrier mobilities and electroluminescence, shown in Figure 4, follow similar trends of previously measured solution-processed films.^[21] At low temperature (77 K), μ_e and μ_h are nearly insensitive to temperature variations up to ≈ 190 K, even when crossing the phase transition between orthorhombic and tetragonal phases at $T \approx 160$ K. At temperatures greater than

190 K both electron and hole mobilities decrease noticeably (Figure 4a). Several processes have been considered to explain the degradation of charge carrier transport in HOIPs at high temperatures, including: i) the structural phase transition to the low mobility tetragonal perovskite crystal structure;^[2,18] ii) the reduced phonon scattering associated with vibrations of the inorganic cage (here PbI₂, relevant only at temperatures below $\approx 160 - 170$ K);^[21] iii) the change in the MA⁺ polarization disorder (for temperatures ranging between 160 and 240 K depending on the measurement technique and perovskite film fabrication conditions);^[21,33,34] iv) electric field screening due to ionic migration.^[2,18,21]

To elucidate the mechanisms underlying the temperature-dependent transport, we extracted the deactivation energy (E_D) of electron and hole mobilities in the low (77 – 213 K) and high (193 – 313 K) temperature ranges. Figure 4b shows the corresponding Arrhenius plots of the mobilities, $\mu(T) = \mu_0 [1 + A \exp(-E_D/k_B T)]$, where μ_0 is the low-temperature mobility, A is a proportionality constant and k_B is the Boltzmann constant. The deactivation energy is found to range from 0.60(± 0.05) eV to 0.15(± 0.02) eV in the high-temperature regime and from 0.024(± 0.024) eV to 0.05(± 0.01) eV in the low-temperature regime for electrons and holes, respectively. These values are consistent with those determined from transient capacitance measurements (0.29 eV and 0.39 – 0.90 eV for the migration

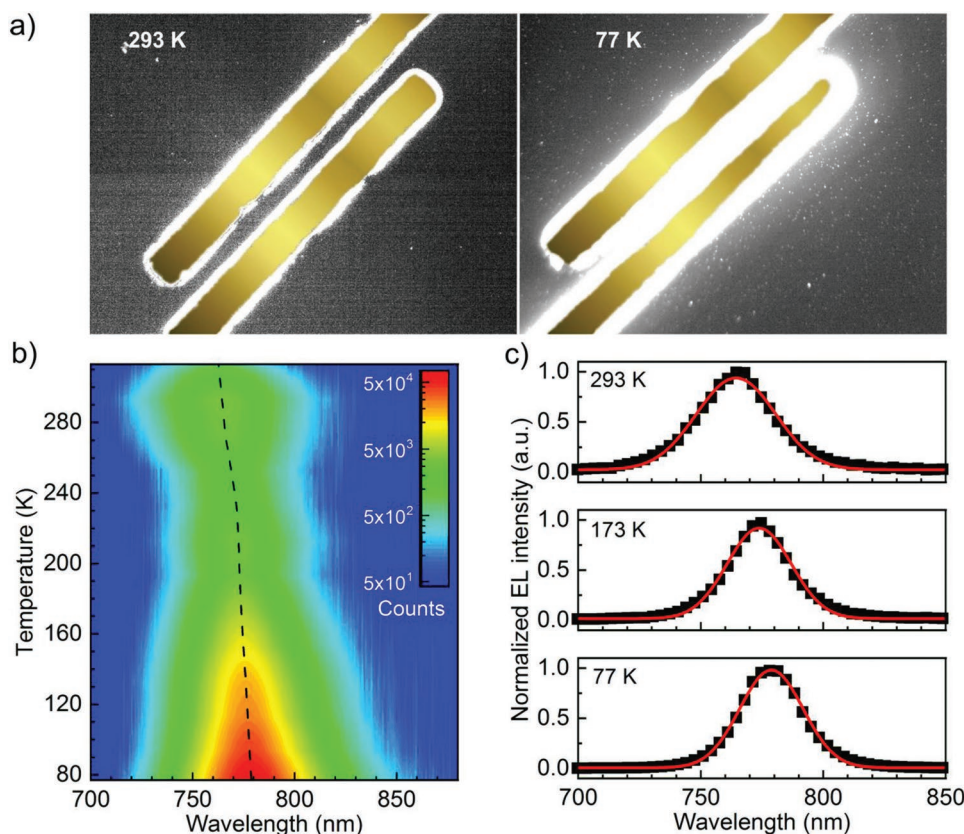


Figure 5. Electroluminescence characteristics of AC-driven PeLETs. a) Optical images of EL emission from PeLET device measured at 293 K and 77 K; b) 2D contour plot of the temperature-dependent emission spectra of the PeLET. The dashed line represents the temperature drift of the EL peak related to the emission from the room-temperature tetragonal phase of the perovskite; c) Normalized EL spectra at representative temperatures below and above the structural phase transition of the perovskite. The spectra were fitted by a single Gaussian peak function (solid lines). All data were collected in AC-driven mode, with $V_{D-S} = -80$ V, $V_{G-S} = \pm 60$ V, and 100 kHz modulation frequency.

of I^- and MA^+ , respectively) as well as theoretical calculations (0.08 – 0.58 eV, 0.46 – 1.12 eV, and 0.80 – 2.31 eV for I^- , MA^+ , and Pb^{2+} , respectively) for different ion migration processes in $CH_3NH_3PbI_3$ thin films.^[34] Thus, even in co-evaporated films, ionic motion appears to remain the primary mechanism limiting transport characteristics of LET devices at high temperatures.

Even though the electron mobility exceeds the hole mobility by more than two orders of magnitude at 77 K, low-temperature electroluminescence characteristics of co-evaporated PeLETs operated in DC-driven mode reveal distinct tunability of the recombination zone, typical of devices operating in the ambipolar regime (Figure 4c). The observed recombination zone is also noticeably wider than in spin-coated devices.^[18] This may be a consequence of the reduced screening deduced from the hysteresis analysis and the nature of negative mobile ions activated at room temperature under positive or negative biasing conditions. Yet the greatest improvement of EL is achieved in AC-driven mode (i.e., with AC bias applied to the gate electrode), which is known to further quench ionic and polarization effects and enhance charge carrier injection via space-charge field-assisted injection nearby the electrodes.^[18,35] Bright light emission from the PeLET operated in AC-driven mode is clearly observed in a wide temperature range from 77 to 313 K,

as shown in Figure 5. Images captured by a CCD camera coupled to the optical microscope show strong and uniform EL, primarily located near the source and drain electrodes (Figure 5a). At low temperature (77 K), the emission completely fills the gap between the top electrodes. Continuous-frame videos showing the variation of EL intensity and position of the emission zone at 77 K and 293 K are provided as Movies S1 and S2, Supporting Information.

Overall, the electroluminescence performance of co-evaporated PeLETs operated in AC-driven mode surpasses all PeLET devices previously made in our laboratories in terms of brightness, uniformity, stability, and operational temperature. Compared to previous spin-coated devices operated under similar conditions, we recorded a noticeable improvement of light-emission characteristics (uniformity of light emission and brightness of the devices—Figure 5b) and enhancement of drain current by two orders of magnitude (Figure S3, Supporting Information), at room temperature, which we have attributed to the better gating performance of the co-evaporated PeLETs. The observation of EL emission up to 313 K is a significant step forward toward practical operation of PeLET devices at room temperature.

Unlike spin-coated devices where the electroluminescence spectra of the PeLET are characterized by distinct excitonic

transitions characteristic of the high-temperature tetragonal and low-temperature orthorhombic phases of the perovskite film, the EL spectra of co-evaporated PeLETs show a dominant emission band centered at 779 nm (at 77 K) (Figure 5b,c). A similar emission spectrum was also observed in DC-driven operation mode. This behavior differs from photoluminescence (PL) and electroluminescence study of spin-coated MAPbI₃ thin films and single crystals, where the structural transition from a low-temperature orthorhombic phase to a high-temperature tetragonal phase can easily be identified.^[2,36–39] The contribution of the orthorhombic phase can also be identified in the low-temperature photoluminescence spectra of our films (Figure S5, Supporting Information). To understand the origin of radiative recombination in PeLETs we analyzed the EL spectra in Figure 5c by a single Gaussian peak fitting approach. A constant hypsochromic shift of the peak maximum position with increasing temperature (marked as black dashed line in Figure 5b) and increase of the full width at half maximum (FWHM) of the peak (from 30 nm at 77 K to 35 nm at 293 K) were observed. Those findings are in line with temperature dependent photoluminescence and absorption measurements in high-temperature tetragonal phase, which implies that EL emission is dominated by the recombination of free excitons in the smaller bandgap tetragonal phase while recombination of bound excitons in orthorhombic phase is negligible.^[37,40] A recent report of ≈10 meV reduction of the exciton binding energy upon heating from 77 K to room temperature^[40] may explain the spectral shift of the EL peak (13 nm, 27 meV) observed in our experiments. It should also be noted that the position of the main EL emission band of thermally co-evaporated PeLETs is slightly shifted toward shorter wavelengths compared to spin-coated devices, which can be attributed to the morphological and structural characteristics of co-evaporated perovskite films, such as their smaller grain size.

The temperature dependence of the EL of co-evaporated PeLET devices reveals a tight interplay between charge carrier transport and ionic screening: the EL intensity decreases upon heating up to 253 K, then suddenly increases up to 293 K, followed by a sharp decrease at higher temperatures (Figure S6, Supporting Information). This behavior is different from spin-coated CH₃NH₃PbI₃ films where a gradual, monotonic decrease of EL with increasing temperature is usually observed.^[18] Here, the initial decrease of EL intensity is in some way related to the activation of nonradiative decay channels, for instance, thermal quenching of electrically generated excitons, as well as the reduction of charge carrier mobility. Indeed, the EL deactivation energy, $E_D = 0.054 \pm 0.003$ eV extracted in the range of 77 – 253 K is comparable to the deactivation energy of the mobility in this temperature range ($E_D = 0.02 - 0.05$ eV). EL activation energy in the second (253 – 293 K) and deactivation energy in third (>293 K) temperature range are estimated to be around $E_A = 0.11 \pm 0.02$ eV and $E_D = 0.8 \pm 0.2$ eV, respectively. The increase of EL near room temperature may be attributed to thermally activated charge carrier release from traps. Based on temperature-dependent spectroscopic studies of charge carrier dynamics in CH₃NH₃PbI₃ films, shallow trap depth for the tetragonal phase is about 20 meV, which is comparable with thermal energy at 293 K, ≈25 meV.^[38] On the other hand, a sharp decrease of light emission at temperatures above 293 K

was also observed in PL measurements, whereas thermal degradation of perovskite was thought to form deep trap states of 1.1 eV depth.^[41] Nevertheless, a tetragonal to cubic phase transition occurring around 310 K may be an alternative mechanism for the EL quenching. Overall, the electroluminescence performance of PeLETs results from the complex interplay of charge carrier injection, radiative and non-radiative recombination processes, and the formation of a depletion layer that screens the applied gating field upon ionic motion. Since the improvement of EL characteristics of co-evaporated PeLETs is not equally observed in DC and AC gating modes, we would exclude carrier injection as the dominant factor. Similarly, charge carrier mobility does not show substantial improvement over the temperature range investigated. Therefore, polarity-dependent deactivation of certain ionic transport channels, likely induced by the better morphology and smaller grain size of the co-evaporated active layers, seems to be responsible for the EL improvement at high temperatures. This is supported by the reduction of hysteresis and the improvement of gating in output characteristics, as well as by the anomalous temperature dependence of EL intensity in the high-temperature regime. As a result, the subtle improvement of co-evaporated MAPbI₃ film morphology, in combination with AC gate bias modulation, is sufficient to achieve PeLET operation at room temperature.

3. Conclusions

In summary, we demonstrated thermally co-evaporated methylammonium lead iodide light-emitting field-effect transistors with balanced ambipolar charge carrier injection and improved electroluminescence characteristics up to room temperature and beyond. The co-evaporated PeLET devices exhibit brighter, more uniform electroluminescence than previous spin-coated devices, especially under AC-driven operation. We attribute the observed performance enhancement to the suppression of ionic contributions in co-evaporated films. These results confirm that improvement in materials quality may allow overcoming the inherent transport limitations arising from ionic effects in metal halide perovskites, toward the use of PeLETs in practical applications such as visual light-communications, solid-state lighting and displays.

4. Experimental Section

Perovskite Preparation and Characterization: The CH₃NH₃PbI₃ perovskite film was deposited on silicon substrates by thermal co-evaporation, following the optimized process described elsewhere.^[24] Substrates were placed at a distance of ≈30 cm from the sources on a plate rotating at 10 r.p.m. The perovskite film was deposited by co-evaporating PbI₂ powder (TCI) and MAI powder (Lumtec) from effusion sources in a high vacuum (pressure <1 × 10⁻⁵ mbar). During the evaporation, the PbI₂ and MAI sources were kept at temperature of 533 K and 373 K, respectively. The total deposition time was around 100 min to obtain a 400 nm thick film. The deposited films were annealed at 373 K for 30 min.

The film morphology was characterized using a scanning probe microscope (Asylum Research/Oxford Instrument Cypher ES) operated in tapping mode and a field-emission scanning electron microscope (JEOL JSM-7600F). AFM images were processed by the Gwyddion

software. The film grain size was determined from the top-view SEM images using the ImageJ software.

PeLET Fabrication and Electrical Measurements: PeLETs were fabricated in a bottom-gate and top-contact configuration on heavily p-doped Si substrates with thermally grown SiO₂ (500 nm) layer as the gate insulator (capacitance of C_i = 6.9 nFcm⁻²). After standard solvent cleaning in an ultrasonic bath, substrates were rinsed in deionized water and dried under a stream of dry nitrogen, followed by UV ozone treatment for 15 min. Afterward, substrates were transferred to the thermal evaporator chamber and 400 nm thick perovskite films were deposited as described above. To complete the device fabrication, 100 nm thick Au electrodes were thermally evaporated through a shadow mask in a high vacuum (≈10⁻⁶ mbar), with a deposition rate of 0.5 Ås⁻¹. To avoid thermal decomposition of the perovskite films, samples were placed on a water-cooled substrate holder kept at 291 K during electrode deposition. The FET channel length (L) and width (W) were 100 μm and 1 mm, respectively. Electrical measurements were carried out at different temperatures ranging from 77 to 313 K, in the dark and under vacuum (≈10⁻³ mbar) using a temperature-controlled probe stage (HFS600E-PB4/PB2, Linkam). DC-driven characteristics were acquired with a 2-channel precision source/measure unit (B2902A, Agilent). Charge-carrier mobilities were extracted from the forward sweeping of transfer characteristics obtained at V_{D-S} = ±60 V, using the conventional equations for metal-oxide semiconductor (MOS) transistors in the

saturation regime: $\mu_{\text{sat}} = \frac{2L}{WC_i} \left(\frac{\partial \sqrt{I_{D-S}}}{\partial V_{G-S}} \right)^2$. For mobility measurements,

at least 3 devices were tested and mean values are presented. The measurement uncertainty was assumed to be the standard deviation of the mean values. The AC-driven measurements were performed applying a square wave bias on the PeLET gate electrode, using an arbitrary waveform generator (Keithley 3390) coupled with a high-voltage amplifier (Falco Systems WMA-300).

EL Measurements: For light emission measurements, PeLETs were operated in both DC- and AC-driven mode. Optical images and videos were taken and acquired by a cooled sCMOS scientific camera (PCO, edge 3.1m) coupled to an optical microscope (Motic PSM-1000). EL spectra were collected using a fiber-coupled spectrometer (Avantes AvaSpec ULS-RS-TEC).

PL Measurements: Temperature-dependent photoluminescence spectra were measured using micro-PL setup (Nikon) combined with a temperature-controlled microscope stage (THMS600, Linkam), under flow of nitrogen to avoid water condensation and degradation of the perovskite film due to moisture absorption. A picosecond laser diode λ = 405 nm (Picoquant P-C-405B) with 40 MHz repetition rate was used as the excitation source. The PL emission was detected by a spectrometer (Acton) combined with a photomultiplier tube.

Supporting Information

Supporting Information is available from the Wiley Online Library or from the author.

Acknowledgements

This research was funded by National Research Foundation, Prime Minister's Office, Singapore under its Competitive Research Programme (CRP Award No. NRF-CRP14-2014-03; Solar CRP: S18-1176-SCR) and by the A*STAR-AME programmatic grant on Nanoantenna Spatial Light Modulators for Next-Gen Display Technologies (Grant No. A18A7b0058).

Conflict of Interest

The authors declare no conflict of interest.

Author Contributions

M.K., A.B., and C.S. conceived the idea. M.K. carried out all electrical and optical measurements and processed the data. L.J. developed and customized the perovskite co-evaporation process with A.B. supervision. M.K. evaporated Au electrodes and made PeLET devices. All the authors contributed to the interpretation of the results. M.K. and C.S. wrote the manuscript. C.S. supervised the work.

Data Availability Statement

The data that support the findings of this study are openly available in NTU research data repository DR-NTU (Data) at <https://doi.org/10.21979/N9/YXYBGB>, and additional data from this study are available from the corresponding author upon reasonable request.

Keywords

AC light-emitting device, co-evaporated perovskite films, light-emitting field-effect transistor, metal-halide perovskites, methylammonium lead iodide

Received: April 19, 2021

Revised: May 21, 2021

Published online: June 10, 2021

- [1] L. Chouhan, S. Ghimire, C. Subrahmanyam, T. Miyasaka, V. Biju, *Chem. Soc. Rev.* **2020**, *49*, 2869.
- [2] X. Y. Chin, D. Cortecchia, J. Yin, A. Bruno, C. Soci, *Nat. Commun.* **2015**, *6*, 7383.
- [3] S. Verlaak, D. Cheyns, M. Debucquoy, V. Arkhipov, P. Heremans, *Appl. Phys. Lett.* **2004**, *85*, 2405.
- [4] A. Jovicic, J. Li, T. Richardson, *IEEE Commun. Mag.* **2013**, *51*, 26.
- [5] J. Zaumseil, *Adv. Funct. Mater.* **2020**, *30*, 1905269.
- [6] C. Eames, J. M. Frost, P. R. F. Barnes, B. C. O'Regan, A. Walsh, M. S. Islam, *Nat. Commun.* **2015**, *6*, 7497.
- [7] J. G. Labram, D. H. Fabini, E. E. Perry, A. J. Lehner, H. Wang, A. M. Glaudell, G. Wu, H. Evans, D. Buck, R. Cotta, L. Echegoyen, F. Wudl, R. Seshadri, M. L. Chabiny, *J. Phys. Chem. Lett.* **2015**, *6*, 3565.
- [8] F. Wang, S. Bai, W. Tress, A. Hagfeldt, F. Gao, *npj Flexible Electron.* **2018**, *2*, 22.
- [9] W. S. Yang, J. H. Noh, N. J. Jeon, Y. C. Kim, S. Ryu, J. Seo, S. Il Seok, *Science* **2015**, *348*, 1234.
- [10] Q. Jiang, Y. Zhao, X. Zhang, X. Yang, Y. Chen, Z. Chu, Q. Ye, X. Li, Z. Yin, J. You, *Nat. Photonics* **2019**, *13*, 460.
- [11] W. Nie, H. Tsai, R. Asadpour, J.-C. Blancon, A. J. Neukirch, G. Gupta, J. J. Crochet, M. Chhowalla, S. Tretiak, M. A. Alam, H. Wang, A. D. Mohite, *Science* **2015**, *347*, 522.
- [12] T. H. Han, S. Tan, J. Xue, L. Meng, J. W. Lee, Y. Yang, *Adv. Mater.* **2019**, *31*, 1803515.
- [13] T. Wu, W. Pisula, M. Y. A. Rashid, P. Gao, *Adv. Electron. Mater.* **2019**, *5*, 1900444.
- [14] A. R. bin M Yusoff, H. P. Kim, X. Li, J. Kim, J. Jang, M. K. Nazeeruddin, *Adv. Mater.* **2017**, *29*, 1602940.
- [15] A. M. Zeidell, C. Tyznik, L. Jennings, C. Zhang, H. Lee, M. Guthold, Z. V. Vardeny, O. D. Jurchescu, *Adv. Electron. Mater.* **2018**, *4*, 1800316.
- [16] W. Yu, F. Li, L. Yu, M. R. Niazi, Y. Zou, D. Corzo, A. Basu, C. Ma, S. Dey, M. L. Tietze, U. Buttner, X. Wang, Z. Wang, M. N. Hedhili, C. Guo, T. Wu, A. Amassian, *Nat. Commun.* **2018**, *9*, 5354.

- [17] H. P. Kim, M. Vasilopoulou, H. Ullah, S. Bibi, A. E. Ximim Gavim, A. G. Macedo, W. J. Da Silva, F. K. Schneider, A. A. Tahir, M. A. Mat Teridi, P. Gao, A. R. B. M. Yusoff, M. K. Nazeeruddin, *Nanoscale* **2020**, *12*, 7641.
- [18] F. Maddalena, X. Y. Chin, D. Cortecchia, A. Bruno, C. Soci, *ACS Appl. Mater. Interfaces* **2018**, *10*, 37316.
- [19] M. U. Chaudhry, N. Wang, K. Tetzner, A. Seitkhan, Y. Miao, Y. Sun, M. C. Petty, T. D. Anthopoulos, J. Wang, D. D. C. Bradley, *Adv. Electron. Mater.* **2019**, *5*, 1800985.
- [20] D. K. Kim, D. Choi, M. Park, K. S. Jeong, J. H. Choi, *ACS Appl. Mater. Interfaces* **2020**, *12*, 21944.
- [21] S. P. Senanayak, B. Yang, T. H. Thomas, N. Giesbrecht, W. Huang, E. Gann, B. Nair, K. Goedel, S. Guha, X. Moya, C. R. McNeill, P. Docampo, A. Sadhanala, R. H. Friend, H. Sirringhaus, *Sci. Adv.* **2017**, *3*, e1601935.
- [22] S. P. Senanayak, M. Abdi-Jalebi, V. S. Kamboj, R. Carey, R. Shivanna, T. Tian, G. Schweicher, J. Wang, N. Giesbrecht, D. Di Nuzzo, H. E. Beere, P. Docampo, D. A. Ritchie, D. Fairen-Jimenez, R. H. Friend, H. Sirringhaus, *Sci. Adv.* **2020**, *6*, eaaz4948.
- [23] J. Ávila, C. Momblona, P. P. Boix, M. Sessolo, H. J. Bolink, *Joule* **2017**, *1*, 431.
- [24] J. Li, H. Wang, X. Y. Chin, H. A. Dewi, K. Vergeer, T. W. Goh, J. W. M. Lim, J. H. Lew, K. P. Loh, C. Soci, T. C. Sum, H. J. Bolink, N. Mathews, S. Mhaisalkar, A. Bruno, *Joule* **2020**, *4*, 1035.
- [25] J. Li, H. A. Dewi, H. Wang, J. H. Lew, N. Mathews, S. Mhaisalkar, A. Bruno, *Sol. RRL* **2020**, *4*, 2000473.
- [26] H. A. Dewi, J. Li, H. Wang, B. Chaudhary, N. Mathews, S. Mhaisalkar, A. Bruno, *Adv. Funct. Mater.* **2021**, *31*, 2100557.
- [27] S. D. Stranks, R. L. Z. Hoyer, D. Di, R. H. Friend, F. Deschler, *Adv. Mater.* **2019**, *31*, 1803336.
- [28] T. Matsushima, S. Hwang, A. S. D. Sandanayaka, C. Qin, S. Terakawa, T. Fujihara, M. Yahiro, C. Adachi, *Adv. Mater.* **2016**, *28*, 10275.
- [29] F. Li, C. Ma, H. Wang, W. Hu, W. Yu, A. D. Sheikh, T. Wu, *Nat. Commun.* **2015**, *6*, 8238.
- [30] M. Sajedi Alvar, P. W. M. Blom, G.-J. A. H. Wetzelaer, *Nat. Commun.* **2020**, *11*, 4023.
- [31] N. Phung, A. Al-Ashouri, S. Meloni, A. Mattoni, S. Albrecht, E. L. Unger, A. Merdasa, A. Abate, *Adv. Energy Mater.* **2020**, *10*, 1903735.
- [32] H. Qiu, J. M. Mativetsky, *Nanoscale* **2021**, *13*, 746.
- [33] A. Bruno, D. Cortecchia, X. Y. Chin, K. Fu, P. P. Boix, S. Mhaisalkar, C. Soci, *Adv. Energy Mater.* **2017**, *7*, 1700265.
- [34] M. H. Futscher, J. M. Lee, L. McGovern, L. A. Muscarella, T. Wang, M. I. Haider, A. Fakharuddin, L. Schmidt-Mende, B. Ehrler, *Mater. Horiz.* **2019**, *6*, 1497.
- [35] X. Liu, J. Kjelstrup-Hansen, H. Boudinov, H. G. Rubahn, *Org. Electron.* **2011**, *12*, 1724.
- [36] H. H. Fang, R. Raissa, M. Abdu-Aguye, S. Adjokatse, G. R. Blake, J. Even, M. A. Loi, *Adv. Funct. Mater.* **2015**, *25*, 2378.
- [37] W. Kong, Z. Ye, Z. Qi, B. Zhang, M. Wang, A. Rahimi-Iman, H. Wu, *Phys. Chem. Chem. Phys.* **2015**, *17*, 16405.
- [38] R. L. Milot, G. E. Eperon, H. J. Snaith, M. B. Johnston, L. M. Herz, *Adv. Funct. Mater.* **2015**, *25*, 6218.
- [39] K. Schötz, A. M. Askar, W. Peng, D. Seeberger, T. P. Gujar, M. Thelakkat, A. Köhler, S. Huettner, O. M. Bakr, K. Shankar, F. Panzer, *J. Mater. Chem. C* **2020**, *8*, 2289.
- [40] T. Meier, T. P. Gujar, A. Schönleber, S. Olthof, K. Meerholz, S. Van Smaalen, F. Panzer, M. Thelakkat, A. Köhler, *J. Mater. Chem. C* **2018**, *6*, 7512.
- [41] A. Al Mamun, T. T. Ava, H. R. Byun, H. J. Jeong, M. S. Jeong, L. Nguyen, C. Gausin, G. Namkoong, *Phys. Chem. Chem. Phys.* **2017**, *19*, 19487.